J Mater Sci: Mater Med (2010) 21:1321–1328
DOI 10.1007/s10856-009-3954-3

In vitro corrosion resistance and cytocompatibility of nano-hydroxyapatite reinforced Mg–Zn–Zr composites

Xinyu Ye · Minfang Chen · Meng Yang · Jun Wei · Debao Liu

Received: 24 August 2009 / Accepted: 25 November 2009 / Published online: 12 December 2009

Abstract Due to good biocompatibility and mechanical properties, magnesium (Mg) and its alloys are considered promising degradable materials for orthopedic applications. In this work, a Mg metal matrix composite (MMC) was fabricated using Mg-2.9Zn-0.7Zr alloy as the matrix and 1 wt% nano-hydroxyapatite (n-HA) particles as reinforcements. In vitro corrosion behavior and cytocompatibility of a Mg–Zn–Zr/*n*-HA composite and a Mg–Zn–Zr alloy were investigated. In contrast with the Mg–Zn–Zr alloy, the MMC has better properties. The average corrosion rate of MMC is 0.75 mm/yr after immersion in simulated body fluid (SBF) for 20 days, and the surface of MMC is covered with white Ca–P precipitates. The electrochemical test results show that the corrosion potential (E_{corr}) of MMC increases to −1.615 V and its polarization resistance (R_p) is 2.56 KΩ with the addition of n-HA particles. The co-cultivation of MMC with osteoblasts results in the adhesion and proliferation of cells on the surface of the composite. The maximum cell density is calculated to be (1.85±0.15) × 10^4/l after 5 days of co-culture with osteoblasts. The average cell numbers for two groups after culturing for 3 and 5 days ($P<0.05$) are significantly different. All the results demonstrate that the Mg–Zn–Zr/*n*-HA composite can be potentially used as biodegradable bone fixation material.

X. Ye · M. Chen · M. Yang · D. Liu
School of Materials Science and Engineering, Tianjin University of Technology, 300384 Tianjin, China

J. Wei
Singapore Institute of Manufacturing Technology, 71 Nanyang Drive, 638075 Singapore, Singapore

D. Liu
Key Laboratory of Display Materials & Photoelectric Devices, (Tianjin University of Technology) Ministry of Education, 300384 Tianjin, China

M. Chen (✉)
Tianjin Key Laboratory for Photoelectric Materials & Devices, 300384 Tianjin, China
e-mail: mfchentj@126.com

1 Introduction

Traditional medical metals and biodegradable polymers are widely used as internal fixation materials [1–3]. However, their applications are limited due to certain disadvantages. Implants such as stainless steel or titanium alloys easily cause stress shielding, and the permanent fixtures need to be removed by a secondary surgery after healing [4]. Degradable polymers exhibit insufficient mechanical properties and the degraded products could cause inflammation [5]. Therefore, it is necessary to develop new degradable materials with adjustable mechanical properties, as well as adequate biocompatibility and biosafety. As potential biomaterials, Mg and its alloys have significant advantages [6–8]. Mg is an essential and harmless element with respect to the human body. The density and Young's modulus of Mg are very close to those of human bone. The density and Young's modulus of Mg are 1.74–2 g/cm^3 and 41–45 GPa, and those of human bone are 1.8–2.1 g/cm^3 and 3–20 GPa. Furthermore, Mg alloys can be dissolved in aqueous solution containing chloride ion, which allows for the degradation in the human body.

Unfortunately, the corrosion rate of Mg is too high to match the growth of new bone. To solve this problem, the addition of alloying elements and surface modification are commonly adopted. For example, LAE442 (Mg-RE alloy) can provide a lower degradation rate in vivo, compared

with AZ31 and AZ91 (Mg–Al alloys) [9]. A hydroxyapatite (HA) coating can slow down the corrosion of AZ91D alloy in simulated body fluid (SBF). The anodic current density of AZ91D increases slowly with a protective HA coating [10]. However, the alloying elements Al and rare earth may cause health problems [7]. In contrast, Mg–Ca alloy [11], which is composed of nutritional elements, has acceptable biocompatibility and biosafety. However, the in vitro corrosion rate of Mg–Ca alloy is faster than Mg alloys containing heavy metal or lanthanon. Furthermore, its elongation is too low to meet the requirements of fracture fixation materials. To improve the properties of Mg alloys, AZ91D/HA composite (MMC-HA) was fabricated by Witte et al. [12]. The results show that the MMC-HA is a cytocompatible material with adjustable mechanical and corrosive properties. However, Al in the matrix is harmful to the nervous system [13]. Micro HA particle conglomerations would also affect the strength and ductility of the MMC-HA composite.

Mg-Zn alloy [14] has good biocompatibility, but its mechanical properties and corrosion resistance may not be satisfied with coarse grains. Usually, the addition of Zr into Mg-Zn alloy can refine grains obviously (Zr > 0.6 wt%) and improve its properties. Although it is not certain when Zr was dissolved as part of the degradation process, it is true that Zr is well tolerated in its solid form. In previous literature, Zr has been adopted as an alloying element in biocompatible Ti alloys [15, 16]. Therefore, we fabricated the Mg–Zn–Zr alloy with 0.7 wt% Zr. Our work aims to develop a new kind of MMC, that of Mg–Zn–Zr alloy and nano-hydroxyapatite (n-HA). By comparing the corrosive and cytocompatible properties of MMC and Mg–Zn–Zr alloy, the new MMC was investigated for its suitability as biodegradable material within bone.

2 Experimental

2.1 Materials and processing

Commercial pure Mg (99.99%) ingot, Zn (99.99%) particles and Mg-Zr master alloy (with 30 wt% Zr) were used as raw materials to form the Mg–Zn–Zr alloy. The gelatin coated n-HA particles with a diameter of about 50 nm and length of about 100 nm were prepared by chemical reaction in the aqueous solutions of $Ca(NO_3)_2$ (100 ml), Gelatin (200 ml) and $(NH_4)_3PO_3$ (100 ml). The chemical deposition was carried out at 90°C, and the pH value was controlled at 9 by the addition of NaOH solution over the course of the reaction. The nominal chemical compositions of the melted Mg–Zn–Zr alloy (sample A1) and Mg–Zn–Zr/*n*-HA composite (sample A2) are listed in Table 1.

To prepare the Mg–Zn–Zr/*n*-HA composite, an array of 10 holes at 10 mm in diameter and 30 mm in depth were drilled evenly into a Mg ingot (about 750 g), then Zn particles and gelatin coated n-HA particles were carefully poured into the holes. Subsequently, the filled Mg ingot and Mg-Zr master alloy were melted in a vacuum induction furnace (ZG-10) with magnetic agitation under argon protection at 720°C. Thereafter, an as-cast ingot of Mg–Zn–Zr/*n*-HA composite measuring 60 mm in diameter was obtained. For comparison, an ingot of Mg–Zn–Zr alloy was also melted using the same parameters. After annealing for 13 h at 420°C, both ingots of Mg–Zn–Zr alloy and Mg–Zn–Zr/*n*-HA composite were hot extruded into bars 8 mm in diameter at 400°C using a YQ32-315 extruder. Then the extruded bars were aged for 24 h at 150°C. The Mg–Zn–Zr alloy and Mg–Zn–Zr/*n*-HA composite samples from extruded and annealed bars were analyzed by wet chemical analysis to characterize the difference between the nominal and actual compositions, and the results are also shown in Table 1. Transmission electron microscopy (TEM, JEM-2010HR, Japan) was used to observe the n-HA particles in the Mg–Zn–Zr/*n*-HA composite.

The samples A1 and A2, which were 8 mm × 3 mm in size, were cut from the extruded and aged bars of Mg–Zn–Zr alloy and Mg–Zn–Zr/*n*-HA composite respectively for in vitro corrosion and cytotoxicity tests. All samples were polished by SiC papers, and then ultrasonically cleaned in acetone, absolute ethanol and distilled water for 10 min respectively.

2.2 Corrosion test

2.2.1 Immersion test

According to ASTM-G31-72 [17], the immersion test was performed in the SBF (pH 7.4) at 37°C by using a WE-3

Table 1 Nominal and analyzed compositions of the materials in this work

Sample index	A1			A2			
Sample description	Mg–Zn–Zr alloy			Mg–Zn–Zr/*n*-HA composite			
	Mg	Zn	Zr	Mg	Zn	Zr	*n*-HA
Nominal compositions (wt%)	Balance	3.0	0.8	Balance	3.0	0.8	1.0
Analyzed compositions (wt%)	Balance	2.9	0.7	Balance	2.9	0.7	No analysis

immersion oscillator. After different immersion periods (3, 7, 10, 15 and 20 days), the samples were removed from the SBF, ultrasonically cleaned in distilled water and dried at room temperature. Field-emission scanning electron microscopy (FE-SEM, JOEL6700F, Japan) was used to characterize the surface morphology of samples A1 and A2 immersed in the SBF. The composition of corrosion products was analyzed by energy dispersive spectrum (EDS). Thereafter, the samples were cleaned using chromic acid to remove the corrosion products before weighing. The corrosion rates were calculated by weight loss according to the following equation:

$$CR = \frac{w}{At\rho} \quad (1)$$

Where CR is the corrosion rate, w is the weight loss, A is the initial surface area exposed to the SBF, t is the immersion time, andρ is the standard density of tested materials (samples A1 and A2). For each type of sample, three tests were conducted and the results were averaged.

2.2.2 *Electrochemical measurements*

A three-electrode cell was used for the measurements, which was set up with a saturated calomel electrode (SCE) reference and a platinum counter electrode. The exposed area of the working electrode (samples A1 and A2) to the solution was 0.3×0.3 cm^2. All the tests were performed in SBF at 37°C in a CHI660C electrochemistry workstation. The polarization scan was carried out from −50 mv to 50 mv at a scan rate of 10 mv/min. Electrochemical impedance spectroscopy (EIS) analyses were performed over a frequency range from 100 kHz to 0.1 Hz. The value of sinusoidal signals was ±10 mv.

2.3 In vitro cell experiment

The osteoblasts were derived from the calvarias bone of newborn Sprague–Dawley (SD) rats and cultured in Dulbecco's modified Eagle's medium (DMEM) containing $NaHCO_3$ and N-2-hydroxyethyl-piperazine-N′-2-ethane-sulfonic acid (HEPES) at 37°C in a saturated humidified atmosphere of 5% CO_2. Cells of second passage were used in this work. According to GB/T16886 [18], a direct contact method was used to determine the cytotoxicity.

Samples A1 and A2 were ultrasonically cleaned by physiological saline for 20 mins, continually rinsed with distilled water, and sterilized using the autoclave at 121°C for 20 mins. After being transferred to a 24-well plate, all samples were covered with 3 ml cell suspension (3.2×10^4 cells/ml) and incubated with 5% CO_2 at 37°C for different culture times (1, 3, 5 and 7 days respectively). PCLM (TE2000-U, Nikon, Japan) was used to investigate the morphology of living cells at the edge of the samples every day. For the proliferation tests, after 1, 3, 5 and 7 days, cells were detached in 0.25% trypsin–EDTA solution and the number of cells in each well was determined with a hemocytocounter. Cellular proliferation assays were performed in quintuplicate. Each data point was presented as means ± deviation (S±D) from five independent experiments. Statistical analysis was carried out using SPSS 11.0 to evaluate the significant cell growth differences on different kinds of materials. Differences were considered significant at $P < 0.05$.

3 Results

3.1 Microstructure of Mg–Zn–Zr/*n*-HA composite

Figure 1 shows the TEM images of sample A2 (transversal section). The refined grains of the Mg–Zn–Zr matrix with a 100–200 nm size were obtained by the extrusion process and dynamic recrystallization (Fig. 1a). In Fig. 1b, two kinds of nano-rods with different colors are uniformly distributed in the grain boundaries of Mg–Zn–Zr alloy. As shown in the HR-TEM images, the interplanar crystal spacing of light-colored particles is 0.35 nm (Fig. 1c) and that of dark-colored particles is 0.42 nm (Fig. 1d), which is consistent with the (002) planes in HA and the (051) planes in MgZn respectively. This demonstrates that the light-colored particles (arrow A) are n-HA rods and the dark-colored particles (arrow B) are the precipitation of MgZn after aging.

3.2 Corrosion test

3.2.1 *Immersion test*

Figure 2 presents the surface morphologies of samples A1 and A2 immersed in the SBF for different periods. At the beginning of immersion (3 days), although some cracks appeared on both surfaces due to the dehydration of the layer in the air, the corrosion product layers of both A1 and A2 appeared to maintain integrity. The cracks on A1 (Fig. 2a) were deeper and wider than the ones on A2 (Fig. 2d). After immersion for ten days, the corrosion layer of sample A1 was undermined and corrosion pits populated its surface (Fig. 2b). In contrast, the surface of sample A2 was still covered by an intact corrosion layer with the appearance of more small cracks (Fig. 2e). At the final immersion time (20 days), the surface of sample A1 was severely destroyed (Fig. 2c). To the naked eye, sample A2 was covered with white precipitates (Fig. 2f) containing C, O, Mg, P and Ca, according to the EDS analysis results (Fig. 3).

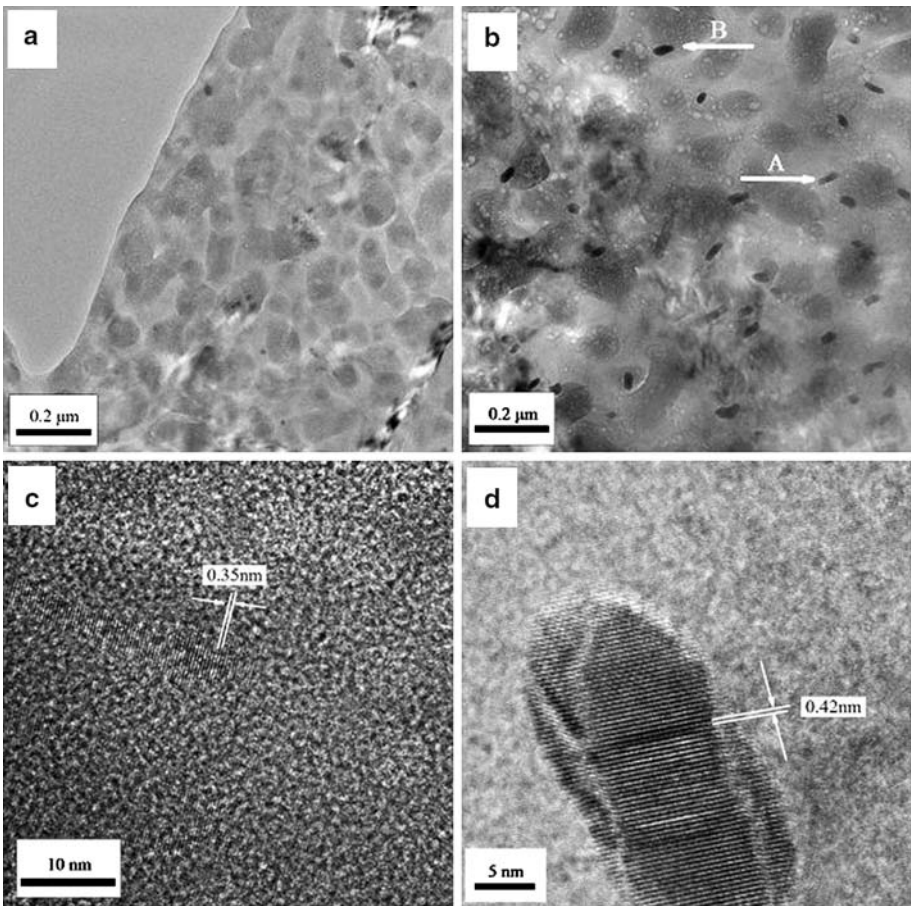

Fig. 1 TEM micrographs of as-extruded composite A2 after aging

Figure 4 shows the corrosion rate of samples A1 and A2. The results reveal that the corrosion rate of two samples decreased with increased immersion time. The average corrosion rate of sample A2 (2.5×10^{-3} mm/d) is much lower than that of sample A1 (5.0×10^{-3} mm/d).

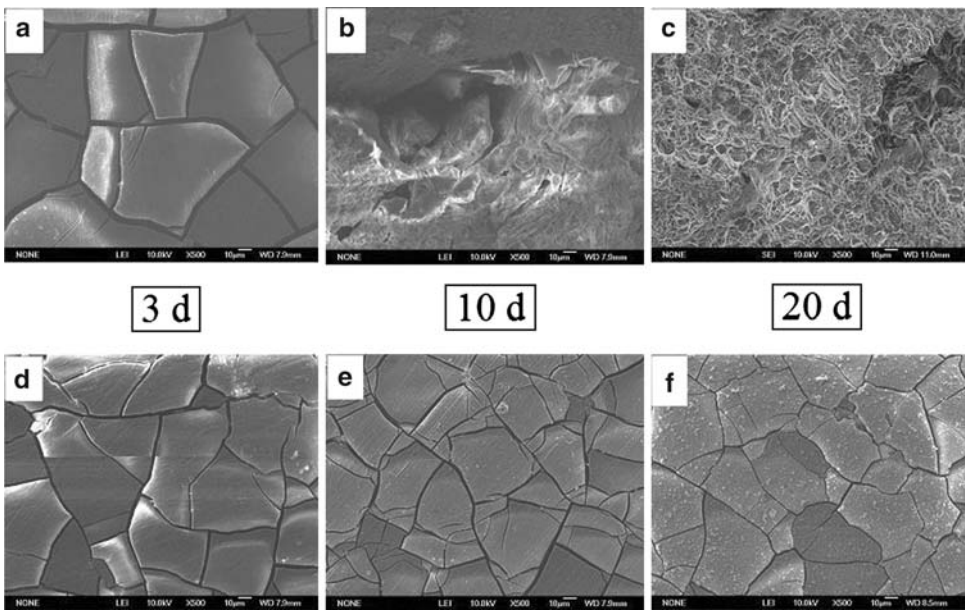

Fig. 2 SEM micrographs of samples A1 (**a-c**) and A2 (**d-f**) after immersion in the SBF for 3, 10 and 20 days

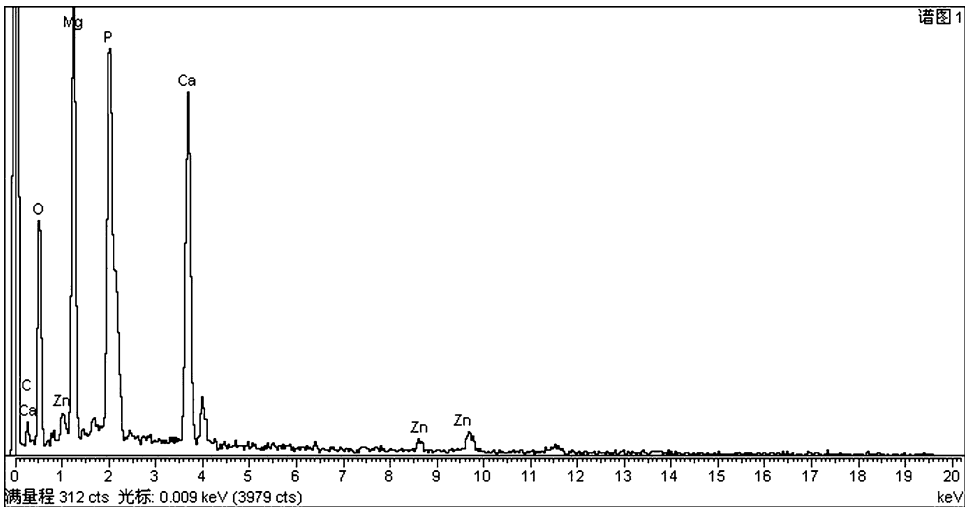

Fig. 3 EDS spectrum of composite A2 after immersion in the SBF for 20 days

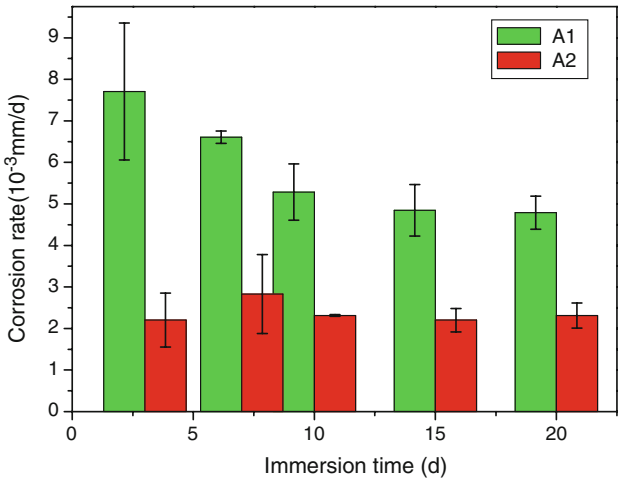

Fig. 4 Corrosion rate of samples A1 and A2 immersed in the SBF

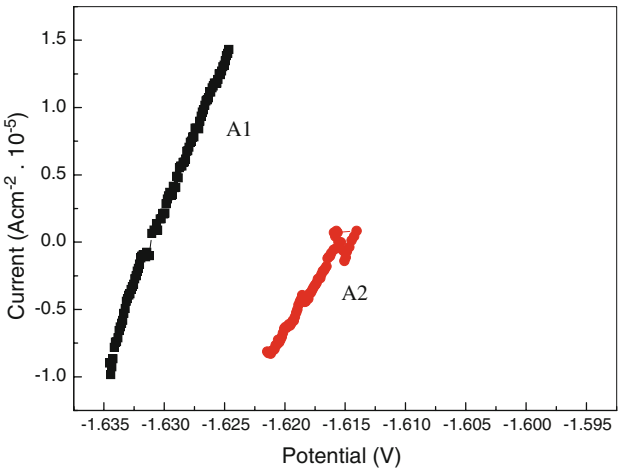

Fig. 5 Linear polarization curves of samples A1 and A2 immersed in the SBF

3.2.2 Electrochemical measurements

The polarization curves of samples A1 and A2 in SBF are shown in Fig. 5. Because the corrosion potential (E_{corr}) of Mg is too negative, linear polarization measurements are adopted in this work. The value of the slope at E_{corr} is the polarization resistance (R_p). Generally, the corrosion rate will decrease with increased E_{corr} and R_p. As shown in Table 2, the corrosion resistance of sample A2 is better than sample A1. This is consistent with the results of the immersion test.

As seen from the Nyquist plots of samples A1 and A2 (Fig. 6), capacitive loops appear at high frequencies and inductive loops appear at low frequencies. For simple comparison, the real impedance at which the imaginary part vanishes for the capacitive part is approximately seen as the charge transfer resistance (Rt). The charge transfer resistance is obtained from the EIS plots. Rt of sample A1 (0.72 KΩ cm^2) is lower than sample A2 (0.76 KΩ cm^2).

Table 2 Summary of corrosion properties of A1 and A2

Samples	E_{corr}(V)	R_p (KΩ)
A1	−1.630	1.63
A2	−1.615	2.56

It also demonstrates that the composite A2 has better corrosion resistance.

3.3 Cytocompatibility test

As shown in Fig. 7, the cell growth of osteoblasts on the surface of each group specimen was evaluated with cell density after culturing for 1, 3, 5 and 7 days. The cell density of osteoblasts is higher on sample A2 as compared to sample A1 for all designated incubation times. It can be concluded that the osteoblasts cultured with sample A2 have a much higher activity rate than sample A1. The

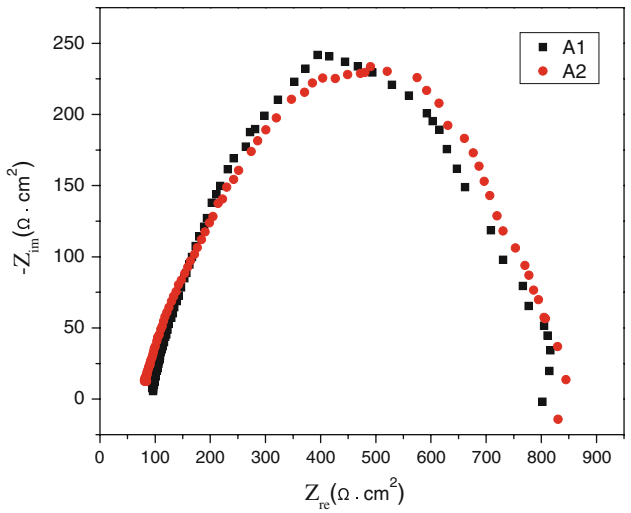

Fig. 6 EIS plots of samples A1 and A2 immersed in the SBF

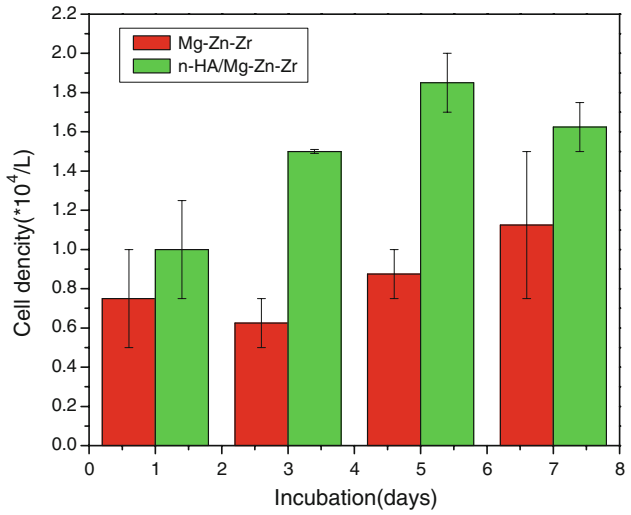

Fig. 7 Cell density of osteoblasts cultured on samples A1 and A2 for various times

maximum cell density on sample A2 was calculated to be (1.85±0.15) × 10^4/l after 5 days of co-culture. Meanwhile, there is a significant difference in the average cell numbers for the two specimens after being cultured for 3 and 5 days ($P < 0.05$).

Figure 8 shows the morphologies of osteoblasts cultured for different time intervals near the samples A1 and A2 respectively. After being cultured for 1 day, almost no cells were attached to the edge of sample A1. Meanwhile, the dissolution appeared in the Petri dishes (area A in Fig. 8a). In the case of sample A2, the cells attached to its edge exhibited the normal form in the shape of a shuttle or elongated polygon (Fig. 8d). After 3 days of co-culture, the cells near both samples A1 and A2 have proliferated, but the number of the cells attached to the side of sample A2 (Fig. 8e) was much higher than that to sample A1 (Fig. 8b). With increased culturing time (5 days), much more dissolution existed around sample A1, which resulted in an increased pH value in the medium and almost no cells could be found by the naked eye (Fig. 8c). In contrast, the cells growing near sample A2 increased significantly and tended to form a cross-linked network (Fig. 8f). In addition, such minor dissolution from sample A2 did not influence the growth and proliferation of cells.

4 Discussion

The results of corrosion tests demonstrate that average corrosion rates of samples A1 and A2 in the SBF are 1.8 mm/yr and 0.75 mm/yr respectively, which are lower than that of the MMC-HA (2.0-3.2 mm/yr) fabricated by a powder metallurgy method [12]. The low corrosion rates are closely related to the grain refinement of samples A1 and A2 after hot extrusion. Previous research revealed that the lower corrosion rate was caused by the low activity of the micro-galvanic battery, which consisted of the matrix and MgZn phase that precipitated along the grain boundary [19]. In this work, the corrosion rate of sample A2 is much lower than that of sample A1 in the SBF, which is explained as follows. The degradation of Mg alloys in the SBF is actually caused by the electrochemical reaction between Mg and water:

$$Mg + 2H_2O = Mg(OH)_2 + H_2 \uparrow \quad (2)$$

At the initial stage of immersion in the SBF, a protective layer of $Mg(OH)_2 \cdot nH_2O$ forms on the Mg alloys, which prevents quick corrosion. Therefore the surfaces of both A1 and A2 exhibited the characteristics of uniform corrosion, and no pitting corrosion was observed. In Fig. 2, the cracks of the $Mg(OH)_2$ layer on sample A1 were wider and deeper than sample A2. This demonstrates that sample A2 corroded more slowly under the same conditions. Obviously, the n-HA particles in composite A2 played an important role in increasing the corrosion resistance of the Mg–Zn–Zr alloy, especially at the later stage of immersion in the SBF.

With the formation of $Mg(OH)_2 \cdot nH_2O$ layer on the samples A1 and A2, acid ions in the SBF such as CO_3^{2-}, PO_4^{3-} and Cl^- were continually adsorbed and the chemical reaction is shown in Eq. 3:

$$Mg(OH)_2 + 2Cl^- \rightarrow MgCl_2 + 2OH^- \quad (3)$$

Because $MgCl_2$ is water soluble, the reaction would undermine the integrity of $Mg(OH)_2$ layer. In addition, pitting corrosion is formed when the Cl^- ions get into the inner part of materials by grain boundary, which accelerates the corrosion of Mg alloys. This is the reason that deep corrosion pits appeared on the surface of sample A1, and the $Mg(OH)_2$ protective layer completely detached after

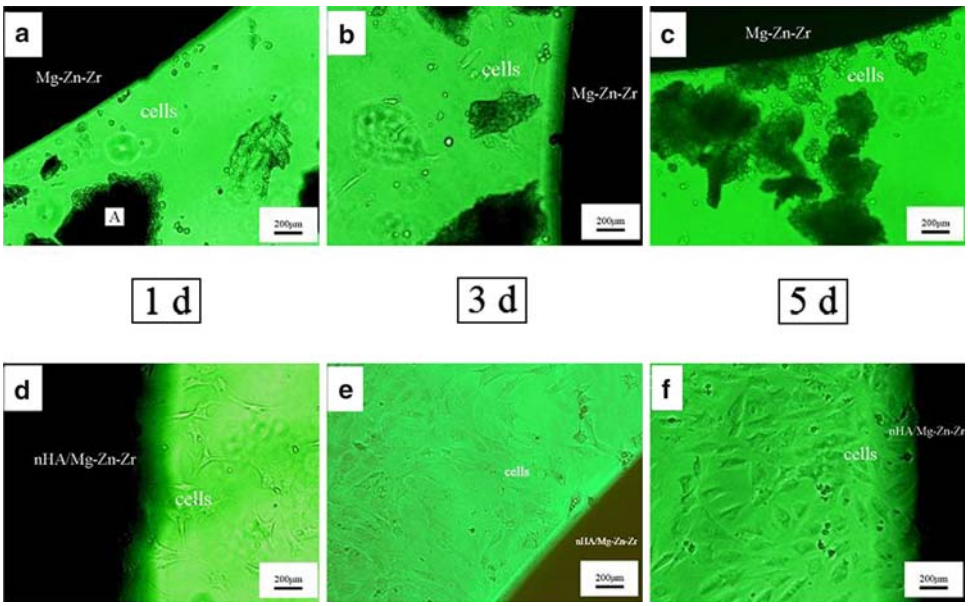

Fig. 8 Optical morphologies of cells cultured on samples A1 (**a-c**) and A2 (**d-f**) for 1, 3 and 5 days. Black areas at the corners of the photographs are the borders and shadows of the test samples. Area A in (**a**) shows the dissolution of sample A1

immersion for 10 days. In contrast, sample A2 was covered with white precipitates that contained Ca and P (Fig. 2f), and no pitting corrosion was observed on the surface. Fig. 1 shows that the n-HA particles in the composite A2 distributed uniformly along the grain boundaries of the Mg–Zn–Zr alloy matrix. These n-HA particles adsorb Ca^{2+} and PO_4^{3-} efficiently and induce the deposition of Ca–P compounds [20]. A new protective layer is gradually formed on sample A2, which will efficiently prevent pitting corrosion because of the Cl^- ions and consequently result in a decreased rate of corrosion. So it is possible to improve the corrosion resistance of Mg alloy composites by adding n-HA particles. This agrees with the results of the electrochemical test.

In vitro responses of osteoblasts to samples A1 and A2 were investigated to confirm their biocompatibility in this work. At the beginning of co-culture, osteoblasts attached to both samples A1 and A2, which demonstrates that these two Mg-based materials show no obvious cytotoxicity. The results agree with work previously published on biomedical Mg alloys. Mg–Ca [11] and Mg–Al-Zn alloys [21] are not cytotoxic in vitro. The in vivo degradation products of Mg-Zn alloys have good biocompatibility with respect to the heart, liver, kidney and spleen [22]. From the comparison of test results, sample A2 exhibits better cytocompatibility than sample A1. Because sample A1 corroded too rapidly, the cells cultured on A1 could not adapt to the medium. After being cultured for 7 days, the pH value of the culturing medium was 9. This is beyond the pH range that is suitable for cell survival. In the case of composite A2 which corroded slowly with the addition of n-HA, the attached cells increased with time. Therefore, Mg-based composite could promote the growth and proliferation of cells if the corrosion rate can be controlled properly. In addition, previous studies reveal that the existence of n-HA particles might contribute to increased cell viability [23]. So adding n-HA particles is a promising way to improve the biocompatibility of Mg-based materials.

5 Conclusions

The Mg–Zn–Zr/*n*-HA composite was synthesized for use as biodegradable material within bone. In contrast with the Mg–Zn–Zr alloy matrix, the Mg–Zn–Zr/*n*-HA composite presents more favorable corrosion resistance and in vitro cytocompatibility properties with the addition of n-HA particles. The average corrosion rate of the composite is 0.75 mm/yr after immersion in the SBF for 20 days. The corrosion potential and polarization resistance increase to −1.615 V and 2.56 KΩ respectively. In vitro cytocompatibility tests reveal the adhesion and proliferation of cells on the surface of the composite. The maximum cell density is $(1.85\pm0.15) \times 10^4$/l after 5 days of co-culture with osteoblasts. Moreover, the average cell numbers for Mg–Zn–Zr alloy and Mg–Zn–Zr/*n*-HA composite are significantly different after culturing for 3 and 5 days ($P < 0.05$).

Acknowledgements This work was supported by Scientific and Technological Item and International Cooperation Item of Tianjin (NO. 07CGHHZ01300), Key Project of Natural Science Foundation of Tianjin and Tianjin Key Subject for Materials Physics and Chemistry.

References

1. Huang JJ, Yang K. Research on magnesium alloys for bio-medical applications. Mater Rev. 2006;20(4):67–9.

2. Gao HM, Chen SJ. Studies of polylactide in internal fixation materials. J Funct Polym. 2004;17(2):281–4.
3. Cui X. Studies of degradable polymers used as bone substitute materials. Chin J Orthop. 2006;14(15):1159–61.
4. Chiu KY, Wong MH, Cheng FT, Man HC. Characterization and corrosion studies of fluoride conversion coating on degradable Mg implants. Surf Coat Tech. 2007;202:590–8.
5. Zou JX, Bai JF, Ye L. The application of polymers in tissue engineering. J Cap Univ Med Sci. 2002;23(4):364–6.
6. Li LC, Gao JC, Wang Y. Corrosion behaviors and surface modification of magnesium alloys for biomaterial applications. Mater Rev. 2003;17(10):29–32.
7. Song GL. Control of biodegradation of biocompatible magnesium alloys. Corros Sci. 2007;49:1696–701.
8. Gurrappa I. Corrosion and its Importance in Selection of Materials for Biomedical Applications. Corros Prevent Control. 2001;48(1):23–7.
9. Witte F, Kaese V, Haferkamp H, Switzer E, Meyer-Lindenberg A, Wirth CJ, et al. In vivo corrosion of four magnesium alloys and the associated bone response. Biomaterials. 2005;26:3557–63.
10. Song YW, Shan DY, Han EH. Electrodeposition of hydroxyapatite coating on AZ91D magnesium alloy for biomaterial application. Mater Lett. 2008;62:3276–9.
11. Li ZJ, Gu XN, Lou SQ, Zheng YF. The development of binary Mg–Ca alloys for use as biodegradable materials within bone. Biomaterials. 2008;29:1329–44.
12. Witte F, Feyerabend F, Maier P, Fischer J, Stormer M, Blawert C, et al. Biodegradable magnesium–hydroxyapatite metal matrix composites. Biomaterials. 2007;28:2163–74.
13. El-Rahman SSA. Neuropathology of aluminum toxicity in rats (glutamate and GABA impairment). Pharmacol Res. 2003;47:189–94.
14. Gu XN, Zheng YF, Cheng Y, Zhong SP, Xi TF. In vitro corrosion and biocompatibility of binary magnesium alloys. Biomaterials. 2009;30:484–8.
15. Lefaix H, Asselin A, Vermaut P, Sautier JM, Berdal A, Portier R, et al. On the biocompatibility of a novel ti-based amorphous composite: structural characterization and in vitro osteoblasts response. J Mater Sci Mater Med. 2008;19:1861–9.
16. Oliveira NTC, Biaggio SR, Rocha-Filho RC, Bocchi N. Electrochemical studies on zirconium and its biocompatible alloys Ti-50Zr at% and Zr-2.5Nb wt% in simulated physiologic media. J Biomed Mater Res. 2005;74A:397–407.
17. Kokubo T, Takadama H. How useful is SBF in predicting in vivo bone bioactivity. Biomaterials. 2006;27:2907–15.
18. Yang XF, Xi TF. Progress in the studies on the evaluation of biocompatibility of biomaterials. J Biomed Eng. 2001;18(1):123–8.
19. Ma YL, Zuo RL, Tang AT, Zhang J, Pan FS. Investigation on alloy phases in As-aged ZK60 magnesium alloy. J Chongqing Univ. 2004;27:91–4.
20. Jonge LT, Leeuwenburgh SCG, Wolke JGC, Jansen JA. Organic–inorganic surface modifications for titanium implant surfaces. Pharmaceut Res. 2008;25:2357–69.
21. Pietak A, Mahoney P, Dias GJ, Staiger MP. Bone-like matrix formation on magnesium and magnesium alloys. J Mater Sci Mater Med. 2008;19(1):407–15.
22. He YH, Tao HR, Zhang Y, Jiang Y, Zhang SX, Zhao CL, et al. The biocompatibility of biological Mg–Zn alloys to the heart, liver, kidney and spleen in vitro. Chin Sci Bull. 2008;53(16):1981–6.
23. Kong LJ, Ao Q, Xi J, Zhang L, Gong YD, Zhao NM, et al. Proliferation and differentiation of MC 3T3-E1 cells cultured on nanohydroxyapatite/chitosan composite scaffolds. Chin J Biotechnol. 2007;23:262–7.